Thermochimica Acta, 34 (1979) 339—356

ON THE USE OF DSC TO ASSESS RADIATION DAMAGE IN ISOTACTIC POLY(METHYL METHACRYLATE)

R.P. KUSY and A R. GREENBERG

Dental Research Center, University of North Carolina, Chapel Hill, N.C. 27514 (U.S.A)

(Received 19 March 1979)

ABSTRACT

Stereoregular poly(methyl methacrylate) (PMMA) was precipitated from solution and subsequently heat-treated to different crystallinities and/or crystal distributions Thereafter, the resulting wafers were exposed either in air or in static vacuum to high-energy γ-radiation via a Cs-137 source. Using DSC the melting temperatures, heats of fusion, and the crystalline fractions were determined for each irradiated sample. By evaluating either the depression of the melting point or the change in the heat of fusion with dose, a relationship was found between the thermodynamic property, on the one hand, and the chemical plus physical changes, i e., G(-units), on the other Present results indicate that G(-units) ~16 and 10, when evaluated from heat of fusion and cryoscopic measurements, vs. 15, 6, or 1.7 obtained by X-ray diffraction, NMR, or gas analysis, respectively No superheating effects were noted in the melting point measurements for heating rates up to 50°C/min The heat of fusion measurements, on the other hand, evidenced a positive correlation, thereby suggesting a G(-units) dependence on heating rate. However, in neither case was reorganization due to premelt recrystallization observed With these newer methods the partition of radiation-induced effects into chemical and physical changes should be possible for polymers which are not labile enough to undergo premelt recrystallization.

INTRODUCTION

A number of techniques have been developed to assess radiation damage in polymers, e g., intrinsic viscosity [1,2], EPR [3], equilibrium swelling [4,5] free-radical scavenging techniques [6], sol—gel partition [7], gas analysis [8,9] and elastic modulus [10]. In some way each of these methods tries to quantify the proportion of chain scissions and/or supramolecular bonds that can result from chemical changes. Since such effects can represent only a portion of the total damage associated with exposure to a radiation field, adjunct techniques must be sought that monitor not only the chemical changes, but also any physical changes that occur, whether or not they are associated with either chain fracture, crosslinking, or recombination sites. Measurements of this more diffuse damage is judged important since, in combination with complex environments and under cyclic stress states, significant reductions of in-service life of a component could result. Consequently, this study presents a new technique, the heat of fusion (ΔH) method, to measure total damage along with a parallel analysis of the more established cryoscopic technique.

EXPERIMENTAL

Sample preparation

One gram of isotactic poly(methyl methacrylate) (PMMA) ($\overline{M}_n \sim 7 \times 10^5$) was crystallized in 20 ml of 4-heptanone by slowly cooling after heating the vessel for 3 days under nitrogen [11,12] After drying in vacuum, the plug that resulted was sectioned into 12-1 mm thick wafers and redried. Following heat treatment (cf. Table 1), the initial crystalline fractions (x_{c_0}) were determined from $x_{c_0} = (\Delta H_0/\Delta H_u)$, in which $\Delta H_u = 1200$ cal mole^{-1} [13] when $x_c = 1.0$ Note that only sample D9 had a bimodal crystalline distribution.

Irradiation

With the exception of D6, all samples were exposed in air in open 2 dram vials to radiation from a Cs-137 γ-ray source at a dose rate of 0.80 Mrad/h at 30°C. On the other hand, D6 samples were irradiated under a static vacuum at less than 10^{-6} Torr in ampules many order of magnitude larger than the sample itself. Each of these samples were opened 2 h post-irradiation and tested immediately No geometric effect in any subsequent measurements was noted, whether a wafer was whole or broken into mg-size pieces. The necessity to report sample geometry and its disposition, the atmosphere and its volume, and the ambient source temperature cannot be overemphasized, since failure to do so can befuddle interpretation [14].

Thermal analysis

Using a Cahn Electro Balance, 2—6 ± 0.01 mg samples were scanned using a Dupont 990 Thermal Analyzer in the DSC mode. The apparatus was calibrated by the specific heat method using both a sapphire disc and Al_2O_3 powder. All runs were made under an atmosphere of 0.2 l Seaford 99.999% pure N_2(g) at 10°C/min, with the exception of sample D12. In this latter case, three additional scanning rates were studied, those of 5, 20, and 50°C/min. From every thermogram, four pieces of information were extracted. The first three, the onset of melting or the low temperature terminus (T_L),

TABLE 1

Initial crystallinities of isotactic PMMA

Sample designation	Special preparation	x_{c_0}
D2,3	Annealed for 1 h at 90°C	0 47
D4,5	None	0 48
D6	Annealed for 1 h at ca. 120°C	0 47
D9	Bimodal distribution formed by partial melting in vacuum at >120°C followed by annealing for 300 h at 80°C	0 33
D10	Partial melt in vacuum for 1 h at 130°C	0.36
D11	Partial melt in vacuum for 1 h at 135°C	0.22
D12	None	0.46

the melting peak (T_M), and the termination of melting (T_U), were determined via constructions of tangents (cf. Fig. 1). The last measurement, the heat of fusion (ΔH), was determined from the ratio of the area (A) contained within the scan and baseline to the mass (m) from the relationship

$$\Delta H(\text{cal mole}^{-1}) = K(MA/m) \tag{1}$$

where K and M are the combined machine constant and the mer molecular weight for PMMA (100 g mole^{-1}), respectively.

Data analysis

Evaluation of the melting point (T_M) data was based on previous experience with cryoscopic measurements. Although DSC does not lend itself to as accurate a determination of the melting peaks as DTA, nevertheless, such measurements may be used since the cryoscopic method requires only that a relative difference persist between "melting points". Moreover, there is no reason why any segment of the crystallite population cannot be monitored, provided proper identification can be made. On this argument both boundaries, T_L and T_U, as well as T_M were evaluated using the Flory equation [15],

$$(1/T) - (1/T_0) = (-R/\Delta H_u) \ln X \tag{2}$$

where the mole fraction of units undamaged (X) times the molar gas constant (R = 2 cal/mole^{-1} K) is proportional to the difference of the reciprocal temperatures initially (T_0) after dose D. Substitution of X into the definition of G(-units), i.e

$$G(\text{-units}) = [(1 - X)/D][(N.10^2)/M.6 \times 10^{19})] \tag{3}$$

yields the number of events occurring per 100 eV of energy absorbed. Here N is Avogadro's number, while 10^2 and 6×10^{19} are factors to convert G(-units) to a 100 eV basis and Mrad to eV, respectively.

On the other hand, ΔH measurements were used to evaluate G(-units) from reasoning similar to that recently used to evaluate X-ray diffraction data [16,17]. On the premise that equal radiation exposure times result in proportional amounts of damage and that the probability of damage in crystalline and amorphous regions is equal [18]

$$G(\text{-units}) \propto -\Delta x_c/(\Delta D \cdot x_{c_0})$$

$$\propto (x_{c_0} - x_{c_F})/(D \cdot x_{c_0}) \tag{4}$$

Substitution of $\Delta H_0/\Delta H_u$ and $\Delta H_F/\Delta H_u$ for the crystallinity yields

$$G(\text{-units}) \propto [1 - (\Delta H_F/\Delta H_0)]/D$$

$$\propto (1 - X)/D \tag{5}$$

in which X equals the fraction of undamaged units, $(\Delta H_F/\Delta H_0)$. Thereby G(-units) may be evaluated from the slope of a $(1 - X)$ vs. D plot and eqn. (3).

RESULTS

Two basic types of DSC scans were observed, a routine endothermic peak (Fig. 1) and a shouldered peak (Fig. 2). The former illustrates the general decrease with dose in both the melting temperatures and the A/m ratios for samples of the same x_{c_0} (Table 1), while the latter documents the suddenness and the extent to which the shoulder can develop. In general, if a shoulder was to form, then it did so by 120—150 Mrad. Moreover, there was a tendency for the shoulder to appear earlier (i.e., at lower doses) as x_{c_0} decreased (e.g , D11 at 40 Mrad). For those specimens irradiated under vacuum (D6 series) vs. air, no unusual differences were noted in either the melting temperatures or the peak areas.

The cumulation of most transition data is tabulated in Table 2. Here two analyses of the same scans are seen for each sample/dose combination, the first of which is illustrated in Fig. 3. There the data of D2—D6 (left) and D10 and 11 (right) are grouped together. From a statistical analysis of these melting point measurements (Table 3), a high level of significance was noted for each regression line. G(-units) was calculated from each line and eqns. (2 and 3) (Table 4). Note the reasonable results obtained using an approximation in which the damage is assumed to be small, i.e., $(1 - X) \leq 0.15$.

Table 5 summarizes the data shown in Figs. 4—6. In the first of these figures, the first column of ΔH was plotted against dose for D2—D6 (top), D10 (middle), and D11 (bottom); then, by utilizing eqn. (5), Figs. 5 and 6 were generated based on the experimentally and the statistically determined ΔH_0 for each wafer. From the least squares data of Table 6, the level of significance of the ΔH data parallels x_{c_0}. This observation is not unexpected, since the experimental error associated with the total thermal analysis procedure (± 60 cal mole^{-1}) increases on a percentage basis with decreasing ΔH. When these five points are combined with the rest of the data base to compute the mole fraction of units changed, a high level of significance was noted. The attempt to circumvent the observation that ΔH_0 was oftentimes

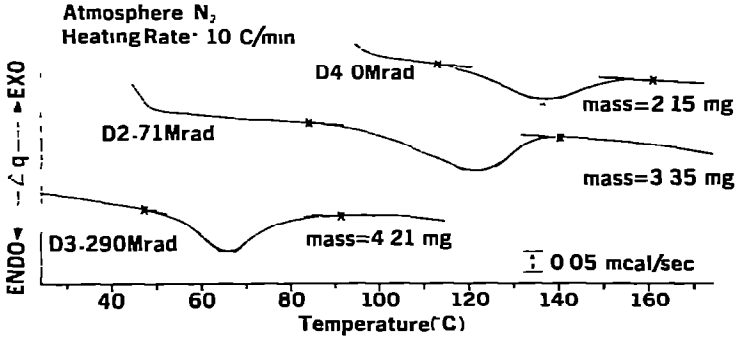

Fig. 1. Typical DSC thermograms of semi-crystalline isotactic PMMA as a function of dose. Crosses designate the onset (T_L) and termination (T_U) of melting via the construction of tangents to the respective baselines, while the intersection of the tangents to the sloping sides of the endotherm define the melting peak (T_M). Initially, $x_{c_0} = 0\ 47$ All samples were irradiated in air.

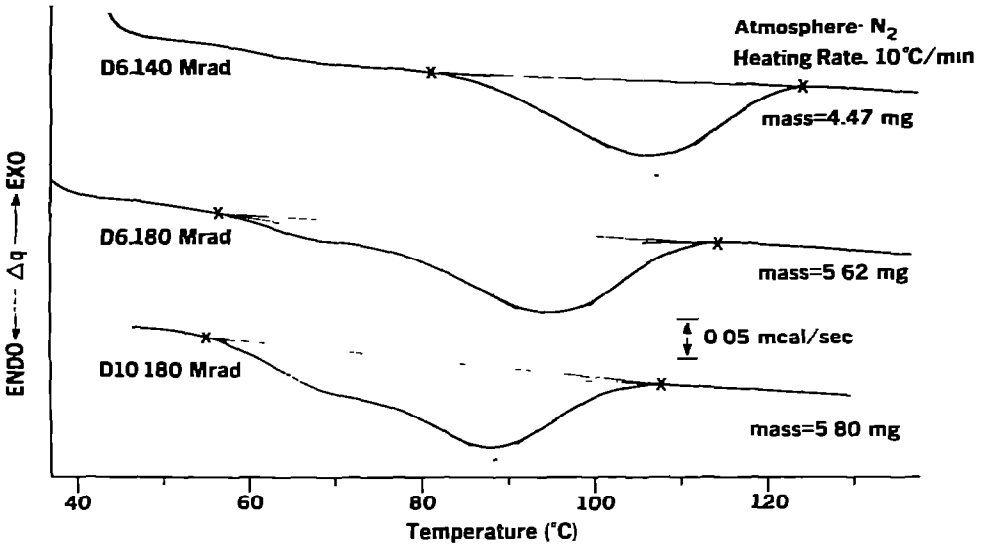

Fig. 2. Development and extent of shoulder formation on the DSC traces of irradiated isotactic PMMA. D6 was irradiated in a static vacuum ($<10^{-6}$ Torr), while D10 was irradiated in air Initially, x_{c_0} = 0 47 and 0 36, respectively.

less than the first irradiated result, by using the intercepts found in Fig 4 to determine $(1 - X)$, yielded no change in the level of significance. What that analysis did do, however, was to shift the central tendency of D11 onto the line and to pass the line nearly through origin. Finally in Table 7, results of G(-units), computed from eqns. (5 and 3) are reported for each set of the ΔH vs. D data shown (cf. Fig. 4), as well as from Figs. 5 and 6. In this way, both the individual sets of experimental results and the statistically biased ΔH_0 data results could be compared with the overall experimental result ((G-units) = 20.8).

Bimodal crystalline distribution

Because the probability of producing crosslinks and chain scissions are different in the crystalline and amorphous regions of certain polymers [19], care has been taken to vary x_{c_0} and its distribution. The rationale is that changing the concentration of amorphous zones and the size and degree of perfection of the crystalline regions, will test the general validity of the technique via modifying the crystalline surface: volume ratio. Figure 7 shows such a change for the case of a bimodal distribution sample, D9 (cf. Table 1). Employing the same geometric constructions described previously (cf. Fig. 1), results of melting point measurements (Table 8) indicate that, although two apparently distinct peaks exist initially, the peaks begin to superimpose even at the lowest dose investigated. As a consequence, the lower terminus of the upper melting peak (T_{U_L}) and the upper extent of the lower transition region (T_{L_U}) become indefinite (Table 8) as the peaks overlap one another. These peaks are not converging, but instead are "filling-in" as they maintain the systematic shift that is associated with the increasing dose (Fig. 8). A statistical analysis of Fig. 8 yields four nearly parallel lines, if

TABLE 2

Summary of melting-point measurements

Sample	Dose (Mrad) [a]	T_U (°C)	T_M (°C)	T_L (°C)
D2	0	155 (156)	136 (137)	101 (104)
D2	35	148 (148)	131 (131)	95 (96)
D2	71	141 (140)	124 (124)	84 (85)
D2	120	125 (125)	109 (109)	66 (68)
D3	200	98 (103)	78 (78)	46 (47)
D3	240	99 (98)	70 (70)	41 (47)
D3	290	89 (91)	65 (65)	47 (47)
D4	0	159 (160)	136 (136)	101 (114)
D4	35	150 (149)	133 (132)	98 (106)
D4	71	141 (140)	125 (125)	91 (91)
D4	120	126 (127)	111 (109)	68 (80)
D4	160	116 (117)	99 (99)	58 (60)
D5	200	104 (103)	77 (77)	44 (46)
D5	240	96 (90)	71 (71)	45 (47)
D5	290	82 (82)	65 (65)	47 (51)
D5	330	79 (78)	61 (61)	42 (48)
D6	0	153 (155)	133 (133)	97 (115)
D6	50	146 (145)	128 (128)	91 (100)
D6	88	137 (137)	123 (122)	78 (77)
D6	140	127 (124)	107 (107)	70 (69)
D6	180	114 (114)	96 (96)	56 (56)
D10	0	166 (161)	140 (139)	118 (118)
D10	40	150 (144)	130 (130)	96 (95)
D10	89	134 (133)	119 (119)	83 (83)
D10	130	123 (123)	104 (104)	73 (73)
D10	180	108 (108)	89 (88)	56 (55)
D11	0	164 (164)	143 (142)	118 (122)
D11	40	153 (150)	134 (134)	96 (96)
D11	89	139 (131)	120 (120)	92 (96)
D11	130	121 (121)	108 (108)	82 (82)
D11	180	105 (104)	91 (91)	67 (67)

[a] 1 Mrad = 6×10^{19} eV/g.

T_{LM} at 0 Mrad is discounted (cf. Table 9). Using these lines, the Flory equation (eqn. 2), and the definition of G(-units) (eqn. 3) yields Table 10. As in Table 4, G(-units) were compared directly (cf. footnote a) and by an approximation (cf. footnote b). By combining all the tabulated data of Tables 4 and 10 for which heating rate (H_r) = 10°C/min, G(-units) values of 10.5 and 11.5, respectively, were obtained. This former value is in good agreement with the cryoscopic results, G(-units) = 12.0 [13,20], obtained previously in the DTA mode at H_r = 20°C/min.

While these thermal measurements had a high level of significance, the ΔH values did not. This deficiency was attributable to the inability to chose a representative baseline prior to peak integration. Using both experimental and least square ΔH_0 values, several computations of G(-units) were made

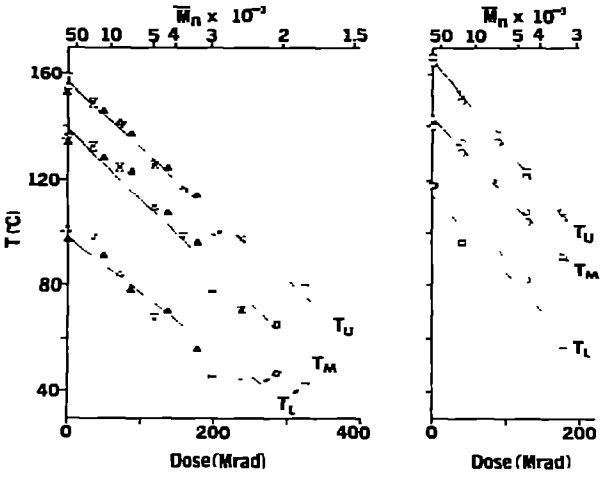

Fig. 3. Depression of melting point (T_M) with dose (cf. Tables 2—4). Left: D2,3 (△); D4,5 (▽); and D6 (▲). Right. D10 (□) and D11 (○) Note that for the same x_{c_0}, the irradiation conducted in vacuum (▲) vs air (△,▽) yielded similar results

TABLE 3

Statistical analysis of melting point measurements

Sample	Linear regression analysis	No. of data points	F_s^d (significant at the 0 001 level)
D2—D6	T_U = 157—0.250D	21	1149
	T_M = 139—0.264D	21	531
	T_L = 98.2—0 210D	21	180
D10,11	T_U = 165—0.332D	10	1262
	T_M = 143—0.292D	10	666
	T_L = 114—0.297D	10	107

[a] Fisher ratio.

TABLE 4

G(-units) as determined from melting-point measurements

Sample		G(-units) [a]	G(-units) [b]
D2—D6	T_U	8.3	8.6
	T_M	9 5	10.0
	T_L	9.2	9.7
D10,11	T_U	10.6	11.2
	T_M	10.3	10.9
	T_L	12.1	12 9

[a] Obtained via eqns. (2 and 3).

[b] Obtained via the approximation, G(-units) $\doteq 10^6\ (\Delta T)\Delta H_u/\mathrm{MRTT}_0$, where $\Delta T = (T_0 - T)/D$.

TABLE 5

Summary of heat of fusion measurements and corresponding mole fraction of crystalline regions damaged

Sample	Dose (Mrad)	ΔH (cal mole^{-1})	$(1-X)$ [a]	$(1-X)$ [b]
D2	0	540 (505)	—	—
D2	35	570 (580)	—0.05	—0.01
D2	71	485 (485)	0.11	0 14
D2	120	440 (400)	0 19	0 22
D3	200	360 (370)	0 33	0.36
D3	240	370 (355)	0.32	0.35
D3	290	260 (270)	0 52	0.54
D4	0	565 (485)	—	—
D4	35	530 (465)	0 06	0.08
D4	71	495 (465)	0.12	0.15
D4	120	425 (370)	0.24	0.27
D4	160	405 (395)	0.28	0 31
D5	200	350 (360)	0.38	0.40
D5	240	360 (330)	0.36	0 38
D5	290	220 (200)	0 61	0 63
D5	330	135 (125)	0.76	0.77
D6	0	525 (525)	—	—
D6	50	545 (505)	—0 04	0.04
D6	88	485 (485)	0 07	0.14
D6	140	330 (310)	0.37	0.42
D6	180	335 (310)	0 36	0.41
D10	0	425 (405)	—	--
D10	40	435 (430)	—0 02	0.01
D10	89	365 (360)	0.15	0.17
D10	130	280 (275)	0.35	0.36
D10	180	315 (300)	0 26	0.28
D11	0	285 (240)	—	—
D11	40	185 (175)	0.35	0 31
D11	89	240 (210)	0.15	0.10
D11	130	250 (245)	0.11	0 06
D11	180	120 (115)	0.57	0.55

[a] Based on the experimental ΔH_0 for each group.
[b] Based on the statistically determined ΔH_0 for each group

from geometric constructions. Three of these representative conventions are illustrated on actual thermograms shown in Fig. 7. On the uppermost scan, an identical construction to that used on all previous results was employed. Here the tangent to the leading and trailing baseline defined the initiation and the termination of melting. By connecting these points (x), the envelope was closed and a G(-unit) ~5 computed according to the procedure outlined earlier. Cognizant that there might well be problems associated with the overlapping endotherms, another convention was attempted. Here the tangents to the "peaks" were extended and a line bisecting these was drawn. From the baseline departure point (x), a second line was drawn perpendicular to the first line. Such a construction was considered analogous to the

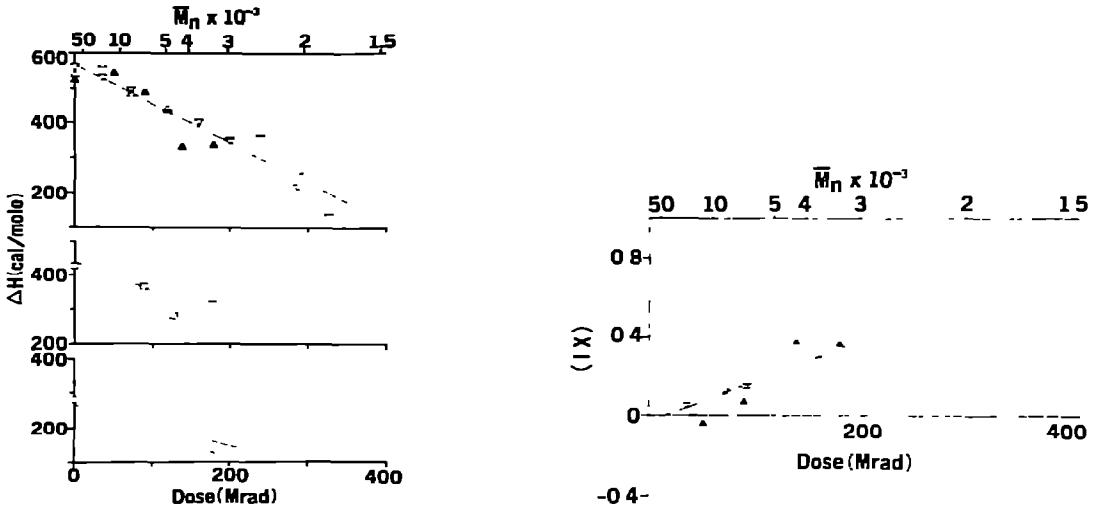

Fig. 4. Regression of the heat of fusion (ΔH) measurements with dose (cf. Tables 5—7).

Fig. 5 Regression of the mole fraction of units damaged ($1 - X$) on dose (D) based on the experimentally determined ΔH_0; cf Tables 5—7)

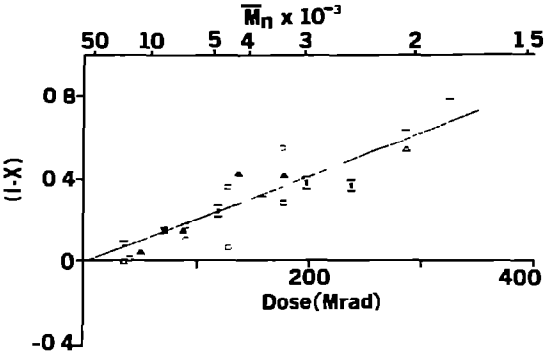

Fig 6. Regression of the mole fraction of units damaged ($1 - X$) on dose (D) (based on the statistically determined ΔH_0; cf Tables 5—7)

TABLE 6

Statistical analyses of heat of fusion measurements

Sample	Linear regression analysis	No of data points	F_s
D2—D6	$\Delta H = 567 - 1.12D$	21	180 [d]
D10	$\Delta H = 438 - 0.848D$	5	9.8 [c]
D11	$\Delta H = 267 - 0.583D$	5	2.2
D2—D6, 10 and 11 [a]	$(1-X) = -0.0299 + 0.00208D$	26	67 [d]
D2—D6, 10 and 11 [b]	$(1-X) = -0.00635 + 0.00204D$	26	77 [d]

[a] Based on the experimental ΔH_0 for each group.
[b] Based on the statistically determined ΔH_0 for each group.
[c] Significant at the 0.05 level
[d] Significant at the 0.001 level

TABLE 7

Computation of G(-units) from heat of fusion measurements

Sample	Regression used	G(-units)
D2,3	ΔH vs. dose	17.3
D4,5		21.0
D6		23 8
D10		19.4
D11		21 9
D2—D6, 10 and 11 [a]	(1—X) vs. dose	20.8
D2—D6, 10 and 11 [b]		20 4

[a] Based on the experimental ΔH_0 for each group.
[b] Based on the statistically determined ΔH_0 for each group.

typical peak areas illustrated in Fig. 1. By assuming that peak separation truly exists for the zero dose peak and that all the lower and all the upper peaks are similar, the outermost halves of each thermogram were proportioned. An evaluation of just the constructed halves and the deduced total peak areas yielded G(-units) of ~5 and ~14, respectively. In spite of the fact that this latter result agrees with the present depression of the melting point data, the premise that similar curve shapes persist with successive dose increments is suspect (e.g., cf. Fig. 2). Finally, constructions similar to the bottommost scan of Fig. 7 were attempted in which the connection of the points marking the departure of tangents from their respective baselines (x) was assumed to represent the best current definition of the overriding baseline (however, cf. Gray [21]). Here the geometric analysis is identical to the uppermost scan except that two vertical lines are now drawn from the intersection of the tangents of each peak to segment ΔH. Since only the relative ratios of ($\Delta H_F/\Delta H_0$) are necessary (cf. eqn. 5), the individual and combined left- and right-hand segments were analyzed. From this last methodology, G(-units) ~40.

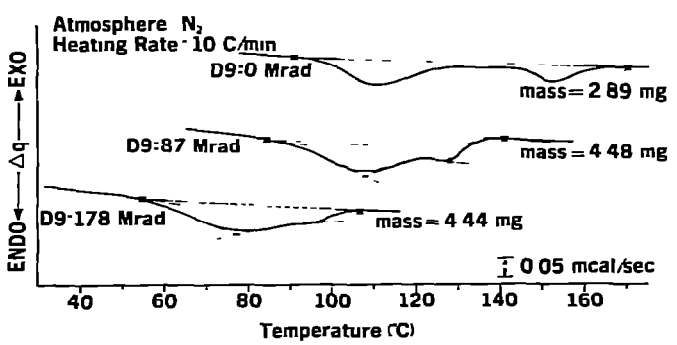

Fig. 7. Annotated DSC scans of the bimodal crystallite distribution of isotactic PMMA illustrating different data interpretation techniques. Initially x_{c_0} = 0.33. All samples were irradiated in air.

TABLE 8

Summary of melting point measurements for the bimodal distribution of sample D9

Dose (Mrad)	T_{U_U} (°C)	T_{U_M} (°C)	T_{U_L} (°C)	T_{L_U} (°C)	T_{L_M} (°C)	T_{L_L} (°C)
0	168	151	140	129	111	103
38	151	139	—	—	119	94
87	140	125	—	—	106	85
130	127	114	—	—	92	69
180	107	97	—	—	80	55

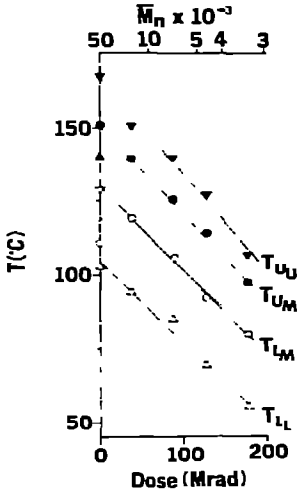

Fig 8. Depression of melting points with dose for the bimodal distribution of sample D9 (cf. Tables 8—10). Closed symbols represent the upper endotherm, while the open symbols signify the lower transition. In general, the symbols ▽, ○ and △ indicate the beginning, peak, or end of the phase transformation. For T_{L_M}, the dashed line represents the statistical analysis of all (○) data, whereas the solid line discounts the 0 Mrad value.

TABLE 9

Statistical analysis of melting point measurements for the bimodal distribution of sample D9

Linear regression analysis	No of data points	F_s (significant at the 0 001 level)
$T_{U_U} = 167—0.328D$	5	277
$T_{U_M} = 151—0\ 299D$	5	1627
T_{L_M} [a] $= 130—0.285D$	4	657
$T_{L_L} = 105—0.272D$	5	232

[a] Deletes T_{L_M} at 0 Mrad.

TABLE 10

G(-units) as determined from melting point measurements of a bimodal distribution of sample D9

	G(-units) [a]	*G*(-units) [b]
T_{U_U}	10 6	12 0
T_{U_M}	10.4	11.6
T_{L_M}	10.8	12 2
T_{L_L}	11.7	13 4

[a] Obtained via eqns. (2) and (3).

[b] Obtained via the approximation, $G(\text{-units}) \doteq 10^6\ (\Delta T)\Delta H_u/\text{MRTT}_0$, where $\Delta T = (T_0 - T)/D$.

Effects of heating rate

The depression of the melting point and the heat of fusion were measured as a function of H_r for D12, a sample similar in crystallinity to D2—D6 (cf. Table 1). For both doses, 0 and 88 Mrad, all thermogram data were again measured by two independent observers (cf. Table 11). Results of the first set of temperature data, shown in Fig. 9, were significant in only two cases (Table 12). From each corresponding pair of melting points, the $(\Delta T/D)$ values were evaluated and *G*(-units) determined via the approximation found in Table 4 (footnote b). Figure 9 shows two *G*(-units) plots — the upper in which the calculated *G* values are based on the extrapolated ΔH_u at a zero heating rate, and the lower in which a unique ΔH_u was determined from a regression of ΔH on H_r (cf. Fig. 10). Both values extrapolated to *G*(-units) ~7—8. (However, the lack of statistical significance in the latter case indicates that there is little functional dependence of y with x, i.e. *G*(-units) is independent of H_r). Finally, in Fig. 10 the plot of ΔH vs. H_r yielded two non-parallel lines for 0 and 88 Mrad, respectively (cf. Tables 11 and 12). From these regression curves, ΔH values were abstracted and used to construct *G*(-units) vs. H_r plot. Note that this Fig had a positive slope, the intercept of which equalled 12.4.

TABLE 11

Summary of thermal measurements for sample D12 as a function of heating rate

Dose (Mrad)	H_r (°C/min)	T_U (°C)	T_M (°C)	T_L (°C)	ΔH (cal mole^{-1})
0	5	154 (154)	136 (136)	104 (104)	510 (475)
0	10 [a]	157 (157)	139 (139)	98 (105)	565 (535)
0	20	153 (153)	127 (127)	95 (95)	595 (580)
0	50	162 (162)	128 (128)	88 (88)	755 (735)
88	5	134 (134)	122 (122)	87 (88)	455 (425)
88	10 [a]	135 (135)	116 (116)	79 (85)	470 (445)
88	20	139 (133)	116 (116)	79 (75)	485 (475)
88	50	144 (145)	122 (123)	76 (75)	530 (510)

[a] Adopted from the combined linear regression analyses of D2—D6

TABLE 12

Statistical analyses of sample D12 as a function of heating rate

Dose (Mrad)	Linear regression analysis		No of data points	F_s
0	T_U	= 153 + 0.162 (H_r)	4	3.8
88	T_U	= 133 + 0 222 (H_r)	4	55 [d]
0	T_L	= 103 — 0.306 (H_r)	4	18 [d]
88	T_L	= 84.0 — 0.177 (H_r)	4	2 7
0	T_M	= 137 — 0 207 (H_r)	4	2 0
88	T_M	= 118 + 0.0615 (H_r)	4	0.29
	G(-units) [a,b]	= 7.48 — 0 0588 (H_r)	12	4.7 [d]
	G(-units) [a,c]	= 7.71 — 0.0141 (H_r)	12	0.17
0	ΔH	= 496 + 5.19 (H_r)	4	143 [d]
88	ΔH	= 450 + 1.62 (H_r)	4	208 [e]
	G(-units)	= 12.4 + 0 436 (H_r)	4	30 [d]

[a] Obtained via the approximation, $G(\text{-units}) = 10^6\ (\Delta T)\Delta H_u/\text{MRTT}_0$, where $\Delta T = (T_0 - T)/D$.

[b] Based on ΔH_u = 1060 cal mole^{-1} at H_r = 0°C/min

[c] Based on ΔH_u = 1110, 1170, 1280, and 1610 cal mole^{-1} for H_r = 5, 10, 20, and 50°C/min, respectively

[d] Significant at the 0.05 level.

[e] Significant at the 0.01 level

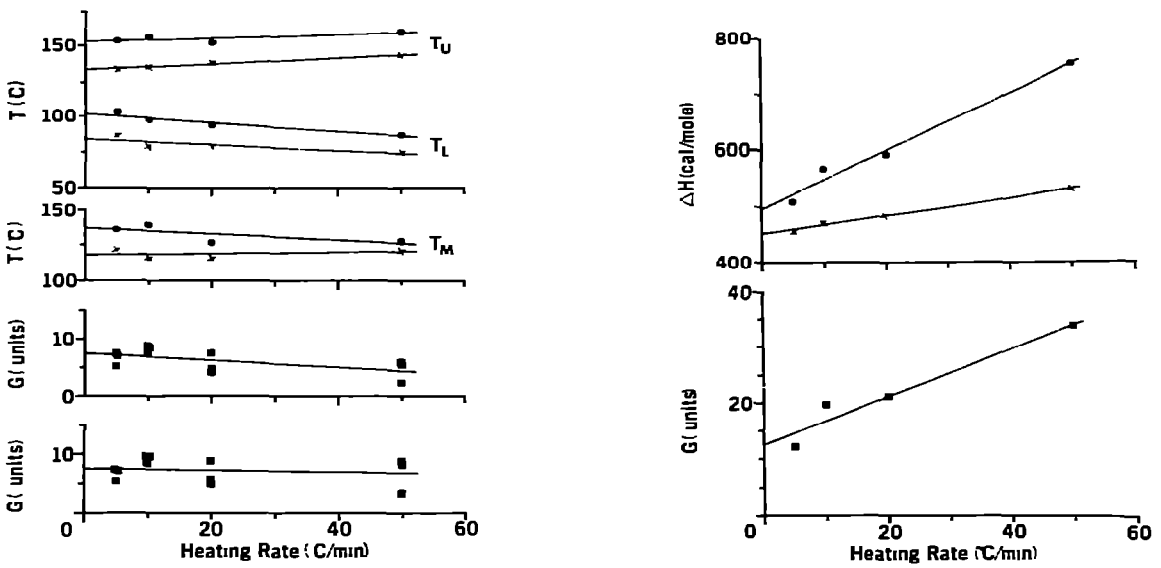

Fig. 9. Influence of heating rate (H_r) on the melting transition and its corresponding G(-units) for sample D12 (cf. Tables 11 and 12). On the upper set of temperature curves, ● and x represent data obtained after irradiation in air to 0 and 88 Mrad, respectively, while the lower curves (■) consider the G(-units) based on an equilibrium value for the heat of fusion and a heating rate dependent heat of fusion (bottom most plot). Initially, $x_{c_0} = 0.46$

Fig 10. The apparent dependence of the heat of fusion (ΔH) and its resultant G(-units) on heating rate (H_r) for sample D12 (cf Tables 11 and 12) ● and x represent thermal data obtained after irradiation in air to 0 and 88 Mrad, respectively.

DISCUSSION

In studying the behavior of irradiated polyethylene over 20 years ago, Dole and Howard [22] noted several factors that could influence the melting range and maximum melting point of a polymer: "(a), the reduction in the melt of the activity of the crystallizing segments by increase of mole fraction of noncrystallizable units such as co-polymer units or units containing branch points, cross-links, and double bonds, or irradiation degradation products, etc.; (b) change in nature of crystallizing units, such as higher molecular weight cross-linked units being the crystallizing substance instead of (in their case) the CH_2 segments of the unirradiated polyethylene; (c), change in crystallite—melt interfacial area per gram of material by disruption of large crystallites into smaller ones [23,24], (d), failure to attain equilibrium between 'pockets' of impurities produced by the irradiation and the main bulk of amorphous material; (e) possibility of simultaneous presence of two kinds of crystallizing segments, either as discrete crystallites or in solid solution". In general, (a) was expected to decrease the melting point; while at higher doses, the opposite effect was likely from (b). Factor (c) was expected to decrease not only the melting point, but also to shift a greater percentage of the crystallites to lower temperatures. Finally since (d) and (e) were postulated to be small, large doses would be required to produce any effects. In the present context Figs. 1 and 2 show the depression of the melting point is accompanied by a corresponding decrease in the heat of fusion. Moreover, in two of the thermograms (cf Fig. 2) a shoulder formed, suggesting an increased disintegration rate of the larger and/or more perfect crystallites. As previously described (cf. Table 1), several wafers were heat treated, varying both the crystalline fraction and distribution. By coincidence, the higher crystallinity material of Fig. 3 (left) had lower melting values than Fig. 3 (right). Apparently there were fewer but more defect free crystals in D10 and D11. Further comparison showed that D10 was 50% more crystalline than D11 (cf. Fig. 4), although their T_M's were essentially the same. Finally, the generation of the bimodal distribution illustrated the greatest variation in crystallite perfection attained (cf. Fig. 7). In spite of all these variations, samples D2—D6 and D9—D11 yielded G(-units) ~9—12 via the melting point depression technique, while samples D2—D6 and 10 and 11 gave G(-units) ~17—24 via the heat of fusion method.

A comparison of the G(-units) determined to date is presented in Table 13. While the present G(-units) ~10 was in general agreement with with previous G(-units) ~12 obtained from cryoscopy [13,20] the mean G(-units) calculated via the heat of fusion method was in better agreement with results found via the X-ray diffraction technique, i.e., G(-units) ~16 vs. 15 [16,17]. The most feasible explanation for this observation was that the definition of what constitutes a crystalline and an amorphous region was not the same This concept of what crystallinity is has been considered in detail by Statton [25], who stated that crystallinity, as judged from X-ray measurements, might differ from results deduced by other methods. For a polymer, then, the gray scale between "the crystalline" and "the amorphous" material might be quite large, and the demarcation lines drawn subject to testing pro-

TABLE 13

Compilation of G(-units) obtained for isotactic PMMA to date

Test method	Previous results	Present results
Gas analysis	1.7 [3,9,30,31]	—
NMR	6 [32]	—
Cryoscopy	12 [13,20]	10,11,8 [a]
X-ray diffraction	15 [16,17]	—
Heat of fusion	—	20,12 [b]

[a] Mean values of data found in Tables 4 (footnote a), 10 (footnote a) and 12 (footnote a and c), respectively.

[b] Representative values for Tables 7 and 12

cedure. While by themselves little significance was attached to the differences between these three methods used to analyze PMMA to date, there is ample information to substantiate that a real difference exists between cryoscopic and heat of fusion measurements. Besides the general observation that the melting range and the peak area under a melting curve are more sensitive to impurities than the actual melting point depression [26], Dole and Howard [22] found for polyethylene irradiated in air in a pile that there was about 70% greater decrease in crystallinity from specific heat measurements than from the depression of the melting point So too, Simon and Rutherford [27] indicated that " . . small amounts of comonomer (butylene or styrene oxide) appear(ed) to disrupt the crystal structure of poly(ethylene oxide) out of proportion to the amount present". Finally in polypropylene exposed in air to Co-60 γ-radiation, Tomlinson and Kline [28] noted tremendous decreases in ΔH that were further enhanced by scanning a second time. Dependent upon which of the two doses were compared with the control material, either 600 or 1800 Mrad, the G(-units) calculated by the ΔH method were from 30—60% greater than those values obtained via the Flory equation. Thus the mole fraction of impurities present may be envisioned as having a sphere of influence that is dependent, in the case of chemical additions, on the nature, quantity, size, and distribution, while in the case of radiation-induced effects dependent on the dose, sample geometry, atmosphere, and ambient source temperature. Clearly T_M must be most concerned with the quantity of defects present while ΔH, in addition, must be concerned with the nature of the region surrounding a defect.

Based on this conclusion, the depression of the melting point should yield values for G(-units) that are comparable with those obtained by methods which measure chemical damage, e.g. gas analysis. In fact these methods do so within a factor of two for the following polymers [29]. polyoxymethylene, polytetrafluoroethylene, poly(ethylene terephthalate), polyethylene, and poly(hexamethylene adipamide). To date, however, three exceptions have been noted [29]: *trans*-1,4-polyisoprene, polypropylene, and isotactic PMMA. Referring to Table 13 once again, one can see that the value of G(-units) ~1.7 obtained by several investigators [3,9,20,31] is 5—10 times less than the present results. This discrepancy can be resolved by observing that a polymer backbone may transform into a row of defects as a result of

the formation of an instantaneous point defect, i.e. fracture, crosslink, or recombination site [17]. In Thompson's NMR work [32], these rows of defects are the isotactic segments that have been randomly converted into syndiotactic or heterotactic configurations, or from one isotactic isomorph to another. Although the NMR could not distinguish the latter, the randomization events leading to syndio- and heterotactic sequences could be evaluated using an analysis similar to the current ΔH method (cf. Fig. 6, ref. 17). By combining value of G(-units) = 6 (Table 13) with the net chemical changes, G(-units) = G(fractures) = 1.7, the quantity of non-crystallizable row and point defects results. The difference between this sum, G(-units) = 7.7, and the cryoscopic measurements might represent the configurational changes to non-crystallizable isotactic isomorphs, in contrast the difference between G(-units) = 7.7 and the G(-units) evaluated by X-ray diffraction and ΔH measurements represents conformational changes associated with the presence of non-crystallizable units.

Because they can affect the magnitude of conformational changes, the phenomena of reorganization and superheating deserve consideration. Wunderlich [33,34] observed that, with increasing heating rates, the T_M of polymer crystallites could increase, decrease, or remain invariant depending upon the particulars of the crystallization process. The resulting effects were largely determined at slow heating rates by the kinetics of reorganization and/or recrystallization, and at faster heating rates by the propensity to superheat. In polytetrafluoroethylene (PTFE) Hellmuth and Wunderlich [35] found that superheating increased with increasing molecular weight, and that the area under the melting curve (i e., ΔH) was heating rate dependent. In another paper by Jaffe and Wunderlich [36] on extended chain crystals of polyoxymethylene exposed to X-radiation, decreasing superheating rates were noted with both increasing dose and heating rate. In Fig. 9 T_L and T_U varied similarly to PTFE (Fig. 3 of ref. 35) with some evidence of superheating and a general broadening of the melting peak. On the other hand, T_M was too erratic to warrant further comment. However, ΔH values (cf. Fig. 10) increased in a manner consistent with the superheating effects cited above The reason for this behavior is not evident. Mass effects [26] were considered negligible since the sample size was quite small (2—6 mg). Although other sources of thermal resistance may have played a role at higher heating rates, an experiment described by O'Neill [37] places doubt on this possibility too. However, his results are inconclusive since the placement of the alumina cloth between the Indium sample and sample holder was heated at only 0.625 K/min. The present viewpoint, then, is that the temperature measurements are genuine, that little reorganization occurs in isotactic PMMA, and that some superheating occurs influencing the ΔH measurements. On this basis G(-units) must be evaluated using the apparent T/D and ΔH_u for each H_r (Fig. 9, bottom). In the absence of knowing the corrected ΔH slopes (Fig. 10, upper), the intercept must be regarded as a conservative estimate. Previous cryoscopic measurements on the influence of heating rate, showed that G(-units) increased nearly 70% for the melting transition of PTFE while no change was noted for the solid-solid transition and the melting transition of PTFE [38] and polyethylene oxide [29],

respectively. In both these experiments the value of G(-units), as extrapolated to $H_r = 0$, was judged best.

SUMMARY

A slow crystallizing polymer, poly(methyl methacrylate) was exposed to γ-radiation and the chemical plus physical changes were determined using DSC. Independent of initial crystallite size and distribution, values of G(-units) were obtained by cryoscopic and ΔH methods that were many times greater than values obtained by chemical analysis. The reportedly simple incidence of chain scission with negligible crosslinking was complicated by significant amounts of racemization. Addition of these so-called line defects to the expected point defects accounted for G(-units) ~8. Differences between this value and the cryoscopic or heat of fusion determinations represent either configurational changes from one isotactic arrangement to another, conformational changes associated with point or line defects, or artifacts associated with reorganization and/or superheating which occurred during the experiment. By controlling these artifacts, more complete understanding of the damage produced by ionizing radiation should result.

ACKNOWLEDGEMENTS

Our thanks to Dr. F.H. Owens for the sample of polymer used in these experiments and to the Physics Department at the University of North Carolina for the use of the Cs-137 source. This investigation was supported by NIH Research Grant No. DE 02668, RCDA No. DE 00052 (R.P.K) and RFA No. DE 05132 (A.R.G.).

REFERENCES

1 P. Alexander, A Charlesby and M Ross, Proc. R. Soc London, Ser. A, 223 (1954) 392.
2 A.R Shultz, P.I. Roth and G.B. Rathmann, J. Polym Sci , 22 (1956) 495.
3 J N. Helbert, P.J Caplan and E H Poindexter, J. Appl. Polym Sci., 21 (1977) 797.
4 P.J. Flory, Principles of Polymer Chemistry, Cornell University Press, Ithaca, N.Y., 1971, pp. 576—581.
5 L E. St. Pierre, H.A. Dewhurst and A M. Bueche, J. Polym Sci., 36 (1959) 105.
6 D.W. Ovenall, J. Chem. Phys , 38 (1963) 2448
7 A. Charlesby and S.H. Pinner, Proc. R. Soc. London, Ser. A, 249 (1959) 367.
8 A Chapiro, Radiation Chemistry of Polymeric Systems, Wiley (Interscience), New York, 1962, pp. 513—515.
9 M. Dole, The Radiation Chemistry of Macromolecules, Vol. II, Academic Press, New York, 1973, pp. 104—108
10 F. Bueche, J. Polym. Sci , 19 (1956) 297.
11 W E. Goode, R.P. Fellman and F.H. Owens, Macromol. Synth , 1 (1963) 25.
12 W E Goode, F.H. Owens, R P. Fellmann, W H. Snyder and J E. Moore, J Polym. Sci , 46 (1960) 317
13 R P. Kusy, J Polym. Sci., 14 (1976) 1527.

14 F.A. Makhlis, Radiation Physics and Chemistry of Polymers, Wiley (Halsted), New York, 1975, pp. 73—81, 105—110, 177—179 and 191—193.
15 P.J Flory, J. Chem. Phys., 15 (1947) 684; 17 (1949) 223.
16 R.P. Kusy and A.R. Greenberg, Macromolecules, 11 (1978) 1051.
17 R.P. Kusy and A.R Greenberg, J. Polym. Sci., in press.
18 P.J. Flory, J. Am. Chem. Soc., 78 (1956) 5222.
19 F.A. Makhlis, Radiation Physics and Chemistry of Polymers, Wiley (Halsted), New York, 1975, p. 158.
20 R.P. Kusy and D T. Turner, J. Polym. Sci., 12 (1974) 2137.
21 A.P. Gray, Polymer Crystallinity Determinations by DSC, communication of the Perkin-Elmer Corporation, 1970.
22 M. Dole and W.H Howard, J. Phys. Chem., 61 (1957) 137.
23 M. Dole, J. Polym. Sci., 19 (1956) 347.
24 P.J. Flory, Trans. Faraday Soc., 51 (1955) 848.
25 W.O. Statton, J. Polym. Sci. Part C, 18 (1967) 33.
26 Thermal Analysis Newsletter. Determination of Purity By Differential Scanning Calorimetry, TAN-5, communication of the Perkin-Elmer Corporation.
27 F.T Simon and J.M Rutherford, Jr., J. Appl. Phys., 35 (1964) 82.
28 J.N. Tomlinson and D.E. Kline, J. Appl. Polym. Sci., 11 (1967) 1931.
29 R.P Kusy and D.T. Turner, Macromolecules, 10 (1977) 493.
30 A. Todd, J. Polym. Sci , 42 (1960) 223.
31 L.A Wall and D.W. Brown, J. Res Natl. Bur. Stand 57 (1956) 131.
32 E.V. Thompson, J. Polym. Sci., Part B, 3 (1965) 671
33 B. Wunderlich, Polymer, 5 (1964) 125, 611.
34 B. Wunderlich, Macromolecular Physics. Crystal Structure, Morphology, Defects, Vol. 1, Academic, New York, 1973, p. 407.
35 E. Hellmuth, B. Wunderlich and J.M Rankin, Jr., Appl. Polym. Symp., 2 (1966) 101.
36 M. Jaffe and B. Wunderlich, J. Polym. Sci., Part A-2,6 (1968) 825.
37 M.J. O'Neill, Anal. Chem., 47 (1975) 630.
38 R.P. Kusy and D.T. Turner, J. Polym Sci , 10 (1972) 1745